^{131}I-labeled monoclonal antibody targeting neuropilin receptor type-2 for tumor SPECT imaging

LICHUN CHEN[1], LIANGLIANG WANG[1], JIANGHUA YAN[2], CHAO MA[1], JING LU[1], GUOQIANG CHEN[1], SHENGYOU CHEN[1], FU SU[1], WEIXING WANG[1] and XINHUI SU[1]

[1]Department of Nuclear Medicine, Zhongshan Hospital Xiamen University, Xiamen, Fujian 361004; [2]Cancer Research Center of Medical School, Xiamen University, Xiamen, Fujian 361102, P.R. China

Received October 20, 2016; Accepted December 5, 2016

DOI: 10.3892/ijo.2016.3808

Abstract. As a co-receptor for vascular endothelial growth factor-3 (VEGF-3), neuropilin receptor type-2 (NRP-2) plays a central role in lymphangiogenesis and angiogenesis. Recently, mounting data of evidence show that NRP-2 is overexpressed in several human cancers, and its overexpression is often associated with poor prognosis. Therefore, it is necessary for us to develop an affinity reagent for noninvasive imaging of NRP-2 expression because it may be possible to provide early cancer diagnosis, more accurate prognosis, and better treatment planning. Due to their high affinity, and specificity, monoclonal antibodies (mAbs) have been considered attractive candidates for targeted cancer therapy and diagnostics. We recently generated and validated a monoclonal antibody that specifically binds NRP-2 b1b2 domain with no cross-reactivity to NRP-1 b1b2 domain, also known to be overexpressed in a variety of cancers. Here, we developed a single photon emission computed tomography (SPECT) probe for imaging NRP-2- positive tumors. Anti-NRP-2 monoclonal antibodies were prepared by hybridomas and were labeled with iodine-131 by chloramine-T method. The *in vitro* physicochemical properties of ^{131}I-anti-NRP-2 mAb was determined. Binding affinity and specificity of ^{131}I-anti-NRP-2 mAb to NRP-2 were assessed using human lung adenocarcinoma A549 cells. Biodistribution and SPECT studies were performed in mice bearing A549 tumor xenografts to evaluate the *in vivo* performance of ^{131}I-anti-NRP-2 mAb. The preparation of anti-NRP-2 mAb was completed successfully by hybridoma with high purity (>95%) and specific for NRP-2 b1b2 domain, but not NRP-1 b1b2 domain. The radiosynthesis of ^{131}I-anti-NRP-2 mAb was completed successfully within 60 min with high labelling efficiency (94.69±3.63%), and radiochemical purity (98.56±0.48%). The resulting probe, ^{131}I-anti-NRP-2 mAb displayed excellent stability in PBS solution during 24-72 h. ^{131}I-anti-NRP-2 mAb showed high binding affinity with A549 cells (96.6±1.44 nM). *In vivo* biodistribution and SPECT studies demonstrated targeting of A549 glioma xenografts was NRP-2 specific. The tumor uptake was 5.86±0.27% ID/g at 6 h, and kept at high level of 4.64±0.82% ID/g at 72 h-post-injection. The tumor to contralateral muscle ratio (T/NT) was 2.08±0.33 at 6 h, and reached the highest level of 3.83±0.18 at 72 h after injection. SPECT imaging studies revealed that ^{131}I-anti-NRP-2 mAb could clearly identify A549 tumors with good contrast, especially at 48-72 h after injection. In conclusion, this study demonstrates that ^{131}I-anti-NRP-2 mAb exhibited highly selective uptake in NRP-2-expressing tumors, and may provide a promising SPECT probe for imaging NRP-2 positive tumors.

Correspondence to: Professor Xinhui Su, Department of Nuclear Medicine, Zhongshan Hospital Xiamen University, 201 Hubin South Road, Xiamen, Fujian 361004, P.R. China
E-mail: suxinhuii@163.com

Key words: monoclonal antibody, neuropilin-2, SPECT, iodine-131

Introduction

Neuropilin (NRP), first identified by Takagi *et al* in 1987 (1), is a 130-140 kDa multifunctional single-spanning transmembrane glycoprotein that plays a central role in neuronal and blood vessel development as receptors for members of the class-3 semaphorin family (SEMAs) of axonal guidance modulators, and also for members of the vascular endothelial growth factor (VEGF) family of angiogenesis stimulators (2-4). Two neuropilin genes, neuropilin-1 (NRP-1) and NRP-2, have been identified. NRP-1 is predominantly expressed in arterial endothelial cells, whereas NRP-2 is preferentially expressed in vein and lymphatic endothelial cells (5). Both NRP-1 and NRP-2 have ~44% amino acid sequence identity and share a similar domain structure, which contains a large extracellular region and a short cytoplasmic tail of ~40 amino acids, lacking any enzymatic activity (3). Their extracellular regions contain three domains: the a1a2 domain is involved in SEMA3-binding, the b1b2 domain is involved in both SEMA3- and VEGF-binding, and the c domain is involved in dimerization (6,7). The binding site for VEGF ligands has been localized to the b1b2 domains of NRP-1 and NRP-2, whereas the binding of semaphorins requires both the a1a2 and b1b2 repeats (8). NRP-1 and NRP-2 interact selectively with different members of the VEGF and semaphorin families and have non-overlapping expression patterns (8). NRP-1 binds VEGF-A165, VEGF-B, VEGF-E, SEMA3A, SEMA3B and SEMA3C, whereas NRP-2 binds VEGF-A165, VEGF-A145, VEGF-C, VEGF-D, SEMA3B,

SEMA3C and SEMA3F (4,8). However, VEGF-A165 binds 50-fold more strongly to NRP-1 than NRP-2 (9). NRP-1 was found to interact with VEGF-A165, and to act as a VEGF co-receptor that specifically enhances VEGFR-2 signaling to promote VEGF biological activity, including endothelial cell migration, sprouting and angiogenesis (6,7). Nevertheless, NRP-2 has different binding preferences for VEGF family members, and is a co-receptor for VEGFR-3 that is involved in lymphatic endothelial cell function (10). Knockout of the NRP-2 gene results in abnormal lymphatic development (11), including an abnormal patterning and marked reduction in small lymphatic vessel and capillaries, supporting a role for NRP-2 in VEGF-C mediated VEGFR-3 signaling and developmental lymphangiogenesis.

Previous studies demonstrated that NRP-1 is expressed on several types of human tumor cells and its expression has been correlated with tumor progression and/or poorer prognosis (3,6,12). Mounting data of evidence suggest that NRP-2 not only plays a central role in lymphangiogenesis, but also in angiogenesis due to a co-receptor for members of VEGF family (13,14). Furthermore, NRP-2 is found to be overexpressed in a variety of human cancers and its upregulation is associated with tumor grade, progression and metastasis, such as lung cancer (15), renal carcinoma (16), pancreatic cancer (17), bladder cancer (18) and colorectal carcinoma (19). Interestingly, the overexpression of NRP-2 is positively correlated with tumor therapy resistance, poor prognosis, and short survival (20,21). Therapeutically targeting NRP-2 expressed in tumor cells using a blocking antibody inhibited the tumor growth and prevented the tumor metastases by blocking the formation of tumor angiogenesis and lymphangiogenesis (19,22). Therefore, NRP-2 has great value as a molecular target for therapeutic intervention, a prognostic indicator of patient survival, and a predictive marker of the response to antineoplastic therapy. Accordingly, NRP-2 inhibition using monoclonal antibodies is considered as a promising strategy for cancer therapy.

In vivo imaging of tumor-receptor offers a more accurate and real-time assay of receptor expression both for patient stratification and monitoring expression-level changes in response to therapy, without such biopsy-associated pitfalls and the need of repetitive invasive biopsies (23). Our previous studies showed that a novel monoclonal antibody against NRP-2 b1b2 domain (anti-NRP-2 mAb), generated by our laboratory (24), can inhibit tumor proliferation, growth, and migration, such as bladder and colorectal cancer (unpublished data), suggesting that anti-NRP-2 mAb may be effective agents for NRP-2-targeted imaging and therapy. Anti-NRP-2 mAb specifically binds to NRP-2 b1b2 domain, but not NRP-1 b1b2 domain, consistent with a previous study (22). Therefore, anti-NRP-2 mAb may be valuable to specifically exploit NRP-2 expression, eliminating any possible undesirable effects mediated by NRP-2. In the present study, we aimed to perform the chloramine-T strategy to label the anti-NRP-2 monoclonal antibody (anti-NRP-2 mAb) with iodine-131, and further determine whether the resulting SPECT (single-photon emission computed tomography) probe ^{131}I-anti-NRP-2 mAb is a suitable agent for imaging mice bearing NRP-2 expression tumors with human lung adenocarcinoma A549 cells.

Materials and methods

General. Chloramine-T was purchased from J&K Scientific, Ltd. (Shanghai, China). The recombinant human peptide sequence of NRP-2 b1b2 was kindly provided by Professor Craig W. Vander Kooi (Department of Molecular and Cellular Biochemistry and Center for Structural Biology, University of Kentucky, Kentucky, USA). Na^{131}I was obtained from the China Institute of Atomic Energy (Beijing, China). Goat anti-mouse IgG antibody was purchased from Santa Cruz Biotechnology, Inc. (Santa Cruz, CA, USA). A PD-10 Sephadex G-25 column from GE Healthcare Bioscience, Ltd. (Diegem, Belgium). rProtein A Sepharose columns were purchased from GE Healthcare Bioscience, Ltd. (Uppsala, Sweden). DMF-96 gamma counter and FCY radioactive chromatography scanner from Hefei Zhongcheng Electromechanical Technology Development Co., Ltd. (Hefei, China). CRC-25R Dose Calibrator from Capintec, Inc. (Ramsey, NJ, USA). SPX-6 SPECT from GE Healthcare Medical Systems, Inc. (Waukesha, WI, USA). Human lung adenocarcinoma A549 cell line, human non-small cell lung carcinoma H1299 cell line, and human normal bronchial epithelial cell line 16HBE were obtained from the Cell Culture Center of Institute of Basic Medical Sciences of Chinese Academy of Medical Sciences (Beijing, China). Female nude mice, 6 and 8 weeks of age, and Balb/c mice were purchased from the Experimental Animal Center of Xiamen University (Xiamen, China).

Cell culture. Two human non-small cell lung carcinoma cell lines (A549, H1299) and a human normal bronchial epithelial cell line 16HBE were cultured in DMEM (Gibco, Grand Island, NY, USA) supplemented with 10% FBS (Gemini, Woodland, CA, USA) and 1% penicillin-streptomycin (Gibco). The cells were maintained in a humidified atmosphere of 5% CO_2 at 37˚C, with the medium changed every two days. A 70-80% confluent monolayer was detached by 0.1% trypsin and dissociated into a single cell suspension for further cell culture.

Quantitative real-time PCR (qRT-PCR). The expression of NRP-2 mRNA in A549, H1299 and 16HBE cell lines is determined by the qRT-PCR based on the method described earlier (12,25). In short, total RNA was isolated with TRIzol reagent (Invitrogen Life Technologies Inc., Grand Island, NY, USA) according to the manufacturer's instructions. The cDNA was synthesized from 2 μg of total RNA using MMLV transcriptase (Toyobo, Shanghai, China) with random hexamers. qRT-PCR were performed using SYBR Premix Ex Taq (Takara, Dalian, China). The human β-actin gene was used as the endogenous control. All cDNA samples were normalized to the β-actin endogenous control; $2^{-\Delta\Delta CT}$ method was used to calculate the relative quantification of NRP-1 mRNA expression. Primers used for real-time PCR are listed in Table I. All qRT-PCRs were performed in duplicate.

Western blot analysis. According to the previously described methods (24), the expression of NRP-2 protein in A549, H1299 and 16HBE cell lines was determined by western blot analysis. Briefly, A549, H1299 and 16HBE cells were lysed in 1 ml RIPA solution (containing 1% Triton X-100, 1% deoxycholate, and 0.1% SDS; Beyotime Biotechnology, Haimen, China)

Table I. Primers for real-time PCR.

Gene	Forward primers	Reverse primers
NRP-2	CACGACTGCAAGTATGACT	TTTTGAGCAATCTTCAGAGC
β-actin	TACCCAGGCATTGCTGACAGG	ACTTGCGGTGCACGATGGA

supplemented with a protease inhibitor (PMSF; Sangon, Shanghai, China) for 30 min at 4˚C, then centrifuged at 12,000 rpm for 30 min at 4˚C to obtain the total cell extracts. Fifteen milliliters of cell extracts was subjected to SDS-PAGE and transferred onto a PDVF membranes by Mini-PROTEAN (Bio-Rad, Hercules, CA, USA). The PDVF membranes were blocked with TBST (10 mM pH 7.4 Tris-HCl, 150 mM NaCl, and 0.1% Tween-20) containing 5% skim milk for 2 h at 37˚C, and incubated overnight at 4˚C with anti-NRP-2 mAb (diluted 1:100). After washed with TBST three times, the membranes were again incubated with goat anti-mouse IgG labeled peroxidase (diluted 1:5,000) for 1 h at 37˚C. Proteins of interest were visualized with ECL in Kodak Image Station 4000R (Carestream Health, Rochester, NY, USA). β-actin was used as an internal control. All experiments were performed in duplicate.

Cellular immunofluorescence staining. Cellular immunofluorescence staining was performed as previously described (12,24). Briefly, the cell-seeded coverslips were washed and fixed. The anti-NRP-2 mAb (diluted 1:100) and fluorescence (TRITC)-labeled secondary antibody (diluted 1:50; Gibco) were added restained with Hoechst 33258 (Beyotime Biotechnology, Jiangsu, China). The slides with cells were incubated without the anti-NRP-2 mAb as control. The fluorescence images were captured at excitation laser of 360 nm and emission laser of 460 nm for Hoechst 33258, and at excitation laser of 488 nm and emission laser of 530 nm for FITC by using Olympus FV 1000 Inverted Confocal Fluorescence Microscope (Olympus, Columbia, SC, USA). All experiments were performed in duplicate.

Immunohistochemical staining (IHC). The expression of NRP-2 in A549 tumor tissues and normal lung tissues was examined by IHC as described previously (12). In brief, the tissue chips were dewaxed and hydrated. Endogenous peroxidase was inactivated with 0.3% H_2O_2 for 10 min. The sections were microwaved for antigen retrieval in 0.01 M citrate buffer (pH 6.0) for 20 min and were incubated with a primary anti-NRP-2 mAb (diluted 1:100) overnight at 4˚C. Subsequently, the sections were incubated with a biotinylated goat anti-rabbit secondary antibody for 30 min at room temperature. Then applying the following steps: color-developing, redyeing, dehydration, making transparent and sealing. The findings of immunostaining were visualized with a Motic AE2000 inverted microscope [Motic (Xiamen) Medical Diagnostic Systems Co., Ltd., Xiamen, Fujian, China].

Production and purification of anti-NRP-2 mAb. Anti-NRP-2 mAb was produced by hybridomas derived from mice immunized with a recombinant human NRP-2 b1b2 in our laboratory according to a method described earlier (24). Briefly, Six-week-old Balb/c mice were injected with hybridoma cells ($2x10^5$-10^6). After 7-10 days, ascites (5-10 ml/mouse) with anti-NRP-2 mAb were collected and centrifuged at 10,000 x g for 15 min to acquire the supernatant. The supernatant was purified by rProtein A sepharose column chromatography according to the manufacturer's protocol to obtain purified anti-NRP-2 mAb. To assess the purity, the purified NRP-2 mAb was subjected to sodium salt-polyacrylamide gel electrophoresis (SDS-PAGE) and was analyzed by Quantity One software (Bio-Rad). The animal procedures were performed according to a protocol approved by the Institutional Animal Care and Use Committee of Zhongshan Hospital Xiamen University.

Analyses for anti-NRP-2-specific antibody and its titer. Indirect ELISA was performed to test anti-NRP-2-specific antibody and its titer according to previously described methods (22,24,26). Briefly, 96-well plates were coated with 10 μg/ml of NRP-2 b1b2 in carbonate buffer (pH 9.6) and incubated overnight at 4˚C. Non-specific binding was blocked with 5% non-fat dry milk in PBS (pH 7.5) for 2 h at 37˚C followed by washing three times with washing buffer (0.05% Tween-20 in PBS). Then the plates were incubated with supernatant of hybridoma cells (ascites) or anti-NRP-2 mAb or anti-NRP-1 mAb (A6-11-26) or antiserum IgG of mice for 2 h at 37˚C, respectively. After washing, the plates were incubated with goat anti-mouse IgG-HRP conjugate for 1 h at 37˚C. Finally, the plates were washed as before and O-phenylenediamine (OPD) was added to develop color. The optical density (OD) was determined at 450 nm by a microplate ELISA reader (Bio-Rad, Tokyo, Japan) after the reaction was stopped with 2 M H_2SO_4. Data were analyzed and graphed with OriginPro 8.1 software (OriginLab, Northampton, MA, USA). All experiments were performed in duplicate.

Labeling anti-NRP-2 mAb with iodine-131. Anti-NRP-2 mAb was labeled with $Na^{131}I$ by the chloramine-T method according to a previous study (27). Briefly, in a 1-ml vial, 100 μg anti-NRP-2 mAb was dissolved in 100 μl 0.01 M phosphate-buffered saline (PBS, pH 7.4), followed by the addition of $Na^{131}I$ (5.5 MBq 25 μl). Then 50 μl chloramine-T (1 mg/ml), freshly prepared in water, was added. The reaction mixture was allowed to stand for 3 min at room temperature. Then reaction was terminated by adding 50 μl of $Na_2S_2O_5$ (2 mg/ml, freshly prepared in water). Radiolabeled antibodies were then purified by size-exclusion chromatography using a PD-10 Sephadex G-25 column. For routine quality control of labeling, the labeling efficiency and radiochemical purity of radiolabeled anti-NRP-2 mAb probes were calculated with TLC method (polyamide film/saline).

In vitro stability analysis. *In vitro* stability in PBS was determined with TLC method (polyamide film/saline) as described with minor modifications (26). Briefly, ^{131}I-anti-NRP-2 mAb (3.11 MBq, 100 μl) was added to 2.0 ml 0.01 M PBS (pH 7.4) and was incubated at 37˚C for 6, 24, 48 and 72 h. At each time-point, 2 μl of the mixture was placed 2 cm above the lower edge and was allowed to evaporate spontaneously, one strip was developed with the mixture developed with saline. After complete development, the paper sheet was removed, dried, and counted in radioactive chromatography scanner. All experiments were performed in duplicate.

Cell assays. Cell uptake and binding affinity assay were performed as previously described with minor modifications (28-30). Briefly, the A549 cells lines were cultured in DMEM supplemented with 10% FBS and 1% penicillin-streptomycin. The cells were maintained in a humidified atmosphere of 5% CO_2 at 37˚C, with the medium changed every two days. A 70-80% confluent monolayer was detached by 0.1% trypsin and dissociated into a single cell suspension for further cell culture.

Cell uptake assays. The A549 cells were washed three times with 0.01 M PBS (pH 7.4) and dissociated with 0.25% trypsin-EDTA. DMEM medium was then added to neutralize trypsin-EDTA. Cells were spun down and re-suspended with serum free DMEM. Cells ($0.5x10^6$) were incubated at 37˚C for 0.5-4 h with $1.11x10^{-2}$ MBq 100 μl ^{131}I-anti-NRP-2 mAb in 0.5 ml serum-free DMEM medium. The non-specific binding of the probes with A549 cells was determined by co-incubation with 10.0 μg unlabeled anti-NRP-2 mAb. At each time-point, the cells were washed three times with chilled PBS and spun down at a speed of 7,000-8,000 rpm. The cell pellets at the bottom of the tube were spliced, and the radioactivity of the pellets was measured using a gamma counter. The uptake (counts/min) was normalized to the percentage of binding for analysis using Excel (Microsoft Software Inc., Redmond, WA, USA). All experiments were performed in duplicate.

Binding affinity assay. The A549 cells ($0.5x10^6$) were plated on 6-well plates one day before the experiment. Cells were washed with PBS three times and incubated at 37˚C for 3 h with $1.11x10^{-2}$ MBq 100 μl ^{131}I-anti-NRP-2 mAb in 0.5 ml serum-free DMEM medium. Non-specific binding of the probes with A549 cells was determined by co-incubation with unlabeled anti-NRP-2 mAb (0.01-10,000 nM final concentration). After incubation, the cells were washed with cold PBS three times and detached with 1 M 0.5 ml NaOH for 5 min. The radioactivity in the cells was measured using a gamma counter and were corrected for physical decay. The data were analyzed using GraphPad Prism (GraphPad Software, Inc., San Diego, CA, USA), and the half maximal inhibitory concentration (IC_{50} value) of ^{131}I-anti-NRP-2 mAb was measured using a least squares fitting routine. All experiments were performed in duplicate.

Biodistribution study. The animal procedures were performed according to a protocol approved by the Institutional Animal Care and Use Committee of Zhongshan Hospital Xiamen University. Cultured A549 cells (~$5x10^6$) suspended in PBS were implanted subcutaneously in the right hind limbs of nude mice. Tumors were allowed to grow to around 0.8-1.0 cm in diameter (7-10 days) and then the tumor-bearing mice were subject to *in vivo* biodistribution and imaging studies.

For biodistribution studies, A549 tumor-bearing mice (n=4 for each group) were injected with ^{131}I-anti-NRP-2 mAb (0.37 MBq, 200 μl) through the tail vein. At 6, 24, 48 and 72 h after injection, the mice were sacrificed, and tumors and normal tissues of interest were removed and weighed, and their radioactivity was measured in a gamma counter. The radioactivity uptake in the tumor and normal tissues was expressed as a percentage of the injected radioactivity per gram of tissue (%ID/g). In order to study the *in vivo* NRP-2 targeting specificity of ^{131}I-anti-NRP-2 mAb, based on the previous studies (44,49), unlabeled anti-NRP-2 mAb (100 μg) was co-injected with ^{131}I-anti-NRP-2 mAb in nude mice bearing A549 tumors (n=4 for each group) via a tail vein, and biodistribution studies were conducted at 48 h after injection.

SPECT imaging. SPECT imaging of tumor-bearing mice was performed on a single-head SPECT scanner with a pinhole collimator. The mice bearing A549 tumor (n=4 for each group) were injected with ^{131}I-anti-NRP-2 mAb (3.7 MBq, 200 μl) with or without co-injection of unlabeled anti-NRP-2 mAb (100 μg) through the tail vein. At 6, 24, 48 and 72 h after injection, the mice were anesthetized with 2% isoflurane and placed on SPECT bed (ventral side down). Whole body static images (200,000 counts) were acquired with a matric of 218x218, and zoom of 2.0. Regions of interest (ROIs) were drawn over the tumor and contralateral muscle, and then the ratio of tumor to contralateral muscle (T/NT) were calculated.

Statistical methods. The experimental data were analyzed by SPSS 18.0 (SPSS Co., Chicago, IL, USA). Statistical analysis was performed using two tailed Student's t-test for unpaired data. Data are expressed as mean ± standard deviation and $P<0.05$ was considered to indicate a statistically significant difference.

Results

Expression of NRP-1 in A549 cell lines and tumor tissue. As shown in Fig. 1A, qRT-PCR results indicated that the expression of NRP-2 mRNA in A549 cells was significantly higher than that in H1299 and 16HBE cells ($P<0.01$). Consistent with qRT-PCR. Western blot analysis (Fig. 2B) demonstrated that A549 cells exhibited higher levels of NRP-2 protein expression ($P<0.05$). Interesting, the expression of NRP-2 in H1299 cells was significantly lower than that in 16HBE cells ($P<0.05$). IHC (Fig. 2) also showed that the expression of NRP-2 is markedly increased in tumor tissue bearing A549, compared to normal mouse lung tissues. Immunofluorescence analysis showed (Fig. 3) that anti-NRP-2 mAb could bind well with NRP-2 receptor on the surface of the A549 cells.

Based on the results we concluded that NRP-2 was overexpressed in the human lung adenocarcinoma A549 cells.

Characterization of anti-NRP-2 mAb. Our previous western blot results showed that anti-NRP-2 mAb was specifically combined with both NRP-2 b1b2 recombinant protein and whole NPR-2 (24). To identify the purity of the current anti-NRP-2

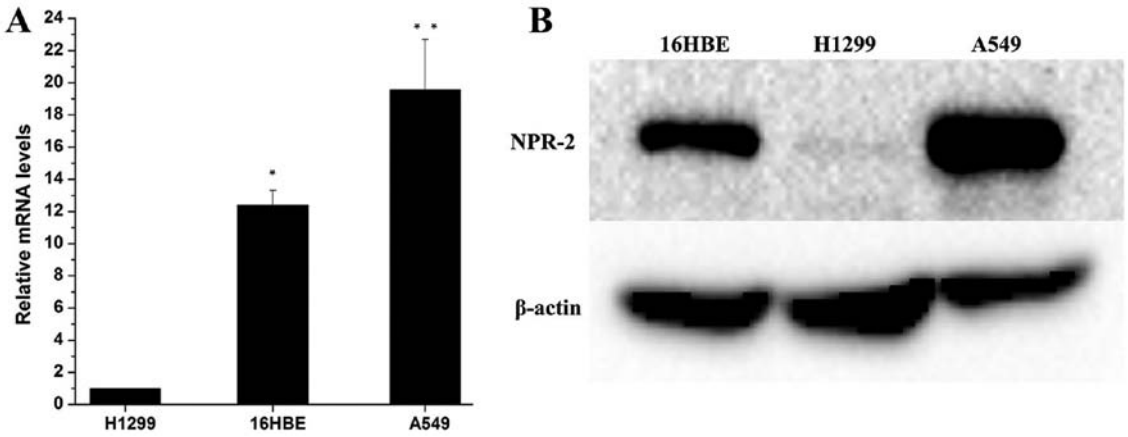

Figure 1. The expression of NRP-2 in two human non-small cell lung carcinoma cell lines (A549, H1299) and a human normal bronchial epithelial 16HBE cell line. (A) The expression of NRP-2 mRNA in these three cell lines. (B) The expression of NRP-2 protein in the three cell lines.

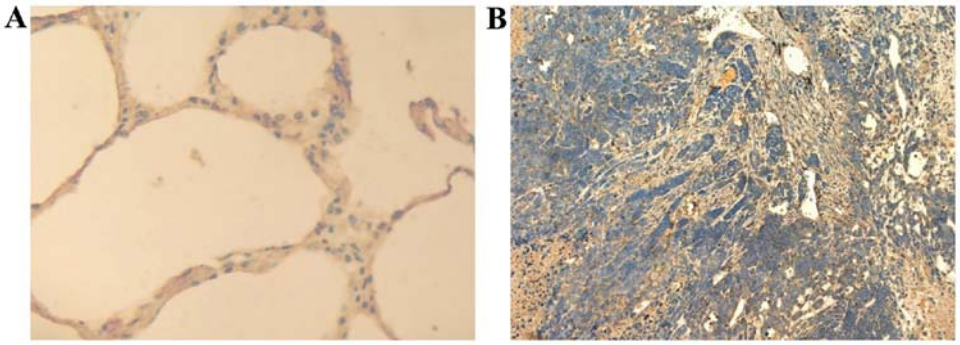

Figure 2. The expression of NRP-2 in (A) normal mouse lung tissues and (B) tumor tissues bearing A549. Original magnification, x100.

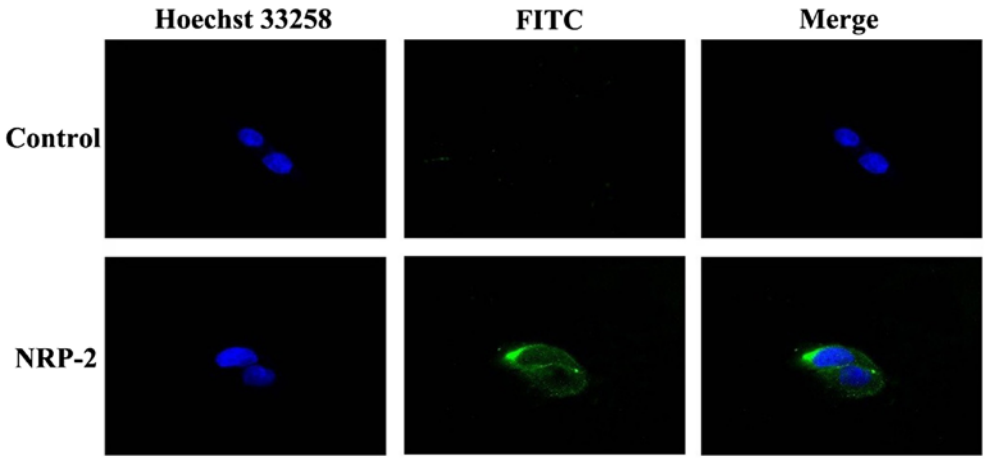

Figure 3. The immunofluorescence of A549 cells.

mAb obtained from ascites, the purified anti-NRP-2 mAb was resolved by an 8% SDS-PAGE gel (Fig. 4). The purity of anti-NRP-2 mAb was determined to be >95%, as detected by Gray analysis of Quantity One 1D-analysis software (GE Healthcare), at a concentration of 2.0 mg/ml. Moreover, the results showed that anti-NRP-2 mAb was IgG1 isotype.

The purified anti-NRP-2 mAb was diluted to measure the titers and specificity against NRP-2 b1b2 by indirect ELISA. As shown in Fig. 5, the purified anti-NRP-2 mAb can bind to synthetic immunogenic peptides with a titer of $2.28x10^5$, and specifically binds to NRP-2 b1b2 domain, but not NRP-1 b1b2 domain.

Radioiodination of anti-NRP-2 mAb. ^{131}I-anti-NRP-2 mAb was successfully radioiodinated. The radiolabeling efficiency, radiochemical purity and specific activity of ^{131}I-A6-11-26 was 94.69±3.63, 98.56 ±0.48 and 162.35±19.6 MBq/μg, respectively.

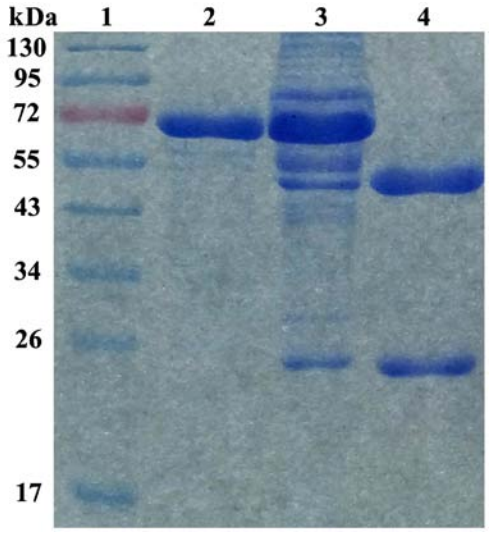

Figure 4. SDS-PAGE analysis of anti-NRP-2 mAb. Lane 1, marker; lane 2, bovine serum albumin (BSA); lane 3, ascites; lane 4, purified NRP2 MAb.

In vitro stability analysis. *In vitro* stability studies (Fig. 6) showed that >85% of ^{131}I-anti-NRP-2 mAb remained intact during 6-72 h of incubation in PBS, indicating that ^{131}I-anti-NRP-2 mAb maintained excellently stable in PBS.

Cell assays. Cell uptake ratios of ^{131}I-anti-NRP-2 mAb are shown in Fig. 7A. ^{131}I-anti-NRP-2 mAb accumulated in A549 cells and reached a highest value of 6.60±0.36% of applied activity at 180 min. When the probe was incubated with large excess of non-radioactive anti-NRP-2 mAb, its uptake levels in A549 cells was significantly inhibited (P<0.05) at all incubation time-points.

The binding affinity of ^{131}I-anti-NRP-2 mAb to NRP-2 was determined through competition binding assays. As shown in Fig. 7B, the IC_{50} value of ^{131}I-anti-NRP-2 mAb was 96.6±1.44 nM.

Overall, these results strongly suggested that ^{131}I-anti-NRP-2 mAb had high NRP-2 binding specificity, affinity in A549 cells, which warranted their further evaluation *in vivo*.

Biodistribution study. At 6, 24, 48 and 72 h after administration, the biodistribution profiles of ^{131}I-anti-NRP-2 mAb are presented in Fig. 8 and Table II, ^{131}I-anti-NRP-2 mAb exhibited high levels of radioactivity accumulation in A549 tumors. At 24 h, the tumor uptake was 5.86±0.27 %ID/g, higher than that in the other organs except for liver (6.22±1.53 %ID/g) and blood (10.93±0.25% ID/g). Moreover, at 72 h, ^{131}I-anti-NRP-2 mAb in the tumor still remained at high level (4.64±0.82% ID/g), significantly higher than that in the other organs including the liver and blood. Lower levels of radioactivity were observed in muscle and bone (1.21±0.16 and 1.18±0.51% ID/g, respectively). The thyroid uptake increased slightly from 0.70±0.05 to 1.33± 0.97% ID/g during 6-72 h post-injection. Furthermore, ^{131}I-anti-NRP-2 mAb provided significantly higher tumor to contralateral muscle ratio (T/NT) and lower tumor-to-blood and tumor to liver ratios (Fig. 9A). At 6 h, the ratio of tumor to contralateral muscle ratio (T/NT=2.08±0.33) was the highest among the tumor to blood (T/B=0.54±0.03), tumor to liver (T/L=0.97±0.22), tumor to kidney (T/K=1.46±0.15), and tumor to lung (T/L=1.37±0.31). Moreover, during 24-72 h, the T/NT ratio increased gradually over time.

Table II. Comparison of biodistribution for ^{131}I-anti-NRP-2 mAb in A549 xenogratfs between 0 μg (unblock) and 100 μg (block).

	^{131}I-anti-NRP-2 mAb (48 h)	
Organ (%ID/g) (Spiked dose)	0 μg (unblock)	100 μg (block)
Tumor	5.12±0.71[a]	2.13±0.09[a]
Heart	2.54±0.31	2.33±0.40
Liver	2.90±0.73	2.10±0.03
Spleen	1.92±0.31	1.63±0.01
Lung	2.22±0.08[a]	1.28±0.03[a]
Kidney	2.65±0.53	2.37±0.04
Stomach	1.31±0.41	1.21±0.06
Bowel	1.58±0.24	1.41±0.18
Bone	1.85±0.43	1.79±0.01
Muscle	1.54±0.15	1.29±0.05
Thyroid	1.15±0.17	1.14±0.05
Blood	5.97±0.34	4.68±0.45
Uptake ratio		
Tumor to blood	0.86±0.07[a]	0.43±0.02[a]
Tumor to Muscle	3.32±0.27[a]	1.66±0.01[a]

Data are mean ± SD, expressed as %ID/g. Student's unpaired two tailed t-test was conducted. [a]P<0.05 comparing 0 μg (unblock) and 100 μg (block) of dose tracer biodistribution at 48 h after injection with ^{131}I-anti-NRP-2 mAb (n=4 for each group).

For *in vivo* blocking study (Table II), ^{131}I-anti-NRP-2 mAb was coinjected with a large excess (100 μg) of the unlabeled anti-NRP-2 mAb to saturate endogenous and overexpressed NRP-2. The co-injection of anti-NRP-2 mAb reduced the uptake in several tissues including liver, kidneys, lung, heart and tumor.

SPECT imaging. SPECT images acquired at 6, 24, 48 and 72 h after injection of ^{131}I-anti-NRP-2 mAb are shown in Fig. 10A. ^{131}I-anti-NRP-2 mAb accumulated in the A549 tumor at 6 h and then showed a gradual increase of uptake. During 24-72 h after injection, A549 tumors were clearly visible, with good tumor to background contrast. When co-injected with unlabeled anti-NRP-2 mAb (100 μg), the tumor was barely visible on SPECT images at 6-72 h after injection (Fig. 10B). Regions of interest (ROIs) analysis of SPECT showed lower ratio of tumor to contralateral muscle (T/NT) for mice injected with 100 μg blocking dose compared to unblocking dose at 6-72 h post-injection (Fig. 9B), especially, at 48 and 72 h after injection (P<0.05).

Discussion

Neuropilin-2 (NRP-2), originally recognized by Chen *et al* (31) in 1997, is a receptor for the secreted semaphorin Sema IV and acts selectively to mediate repulsive guidance events in

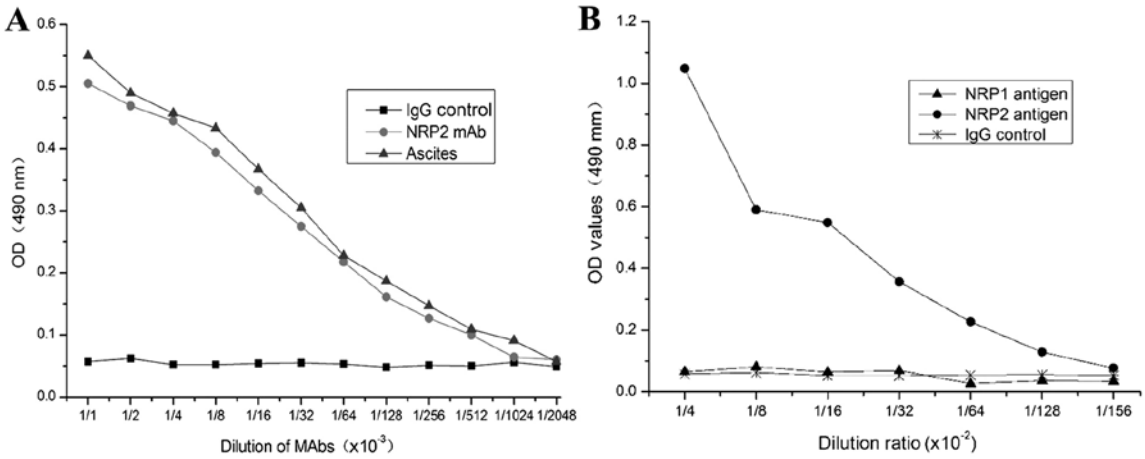

Figure 5. Titer analysis of (A) anti-NRP-2 mAb and specificity against (B) NRP-2 b1b2.

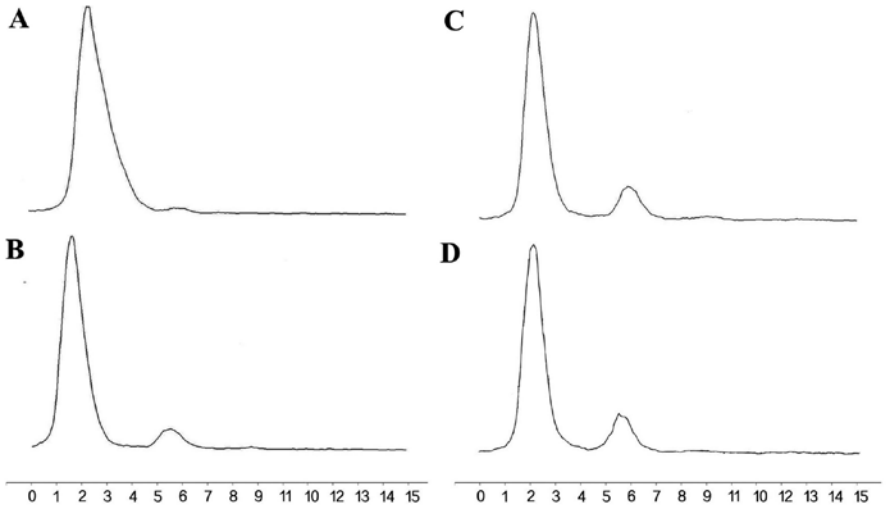

Figure 6. TLC radiochromatograms of purified (A) ^{131}I-anti-NRP-2-mAb and radiolabeled probe after (B) 24 h, (C) 48 h and (D) 72 h of incubation with PBS.

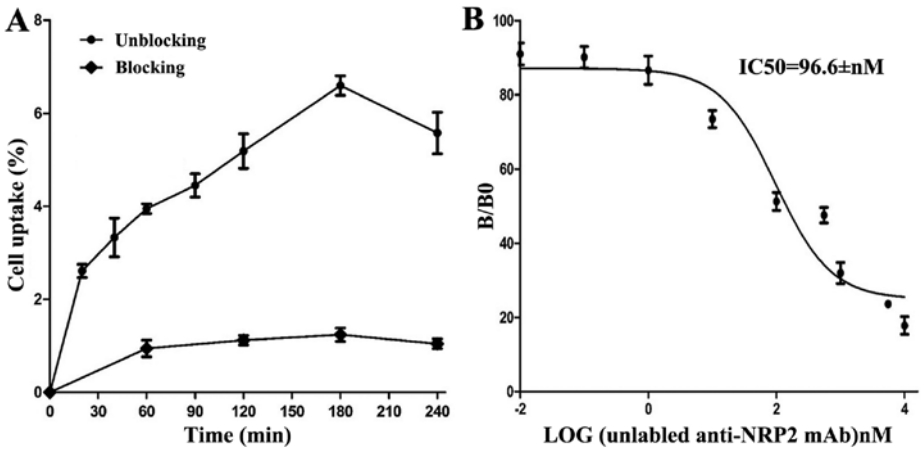

Figure 7. (A) Uptake and (B) binding affinity assay of ^{131}I-anti-NRP-2 mAb in A549 cells.

discrete populations of neurons. Subsequently, NRP-2 was found to be expressed in venous and lymphatic endothelial cells and, upon ligand stimulation (such as semaphorin 3F, VEGF-C and VEGF-A), induces neural development and the growth of newly formed blood and lymphatic vessels, and increases survival and migration of vascular and lymphatic endothelial cells (12,14). Interestingly, NRP-2 is also expressed in several human tumor cells and tissues, and is involved in

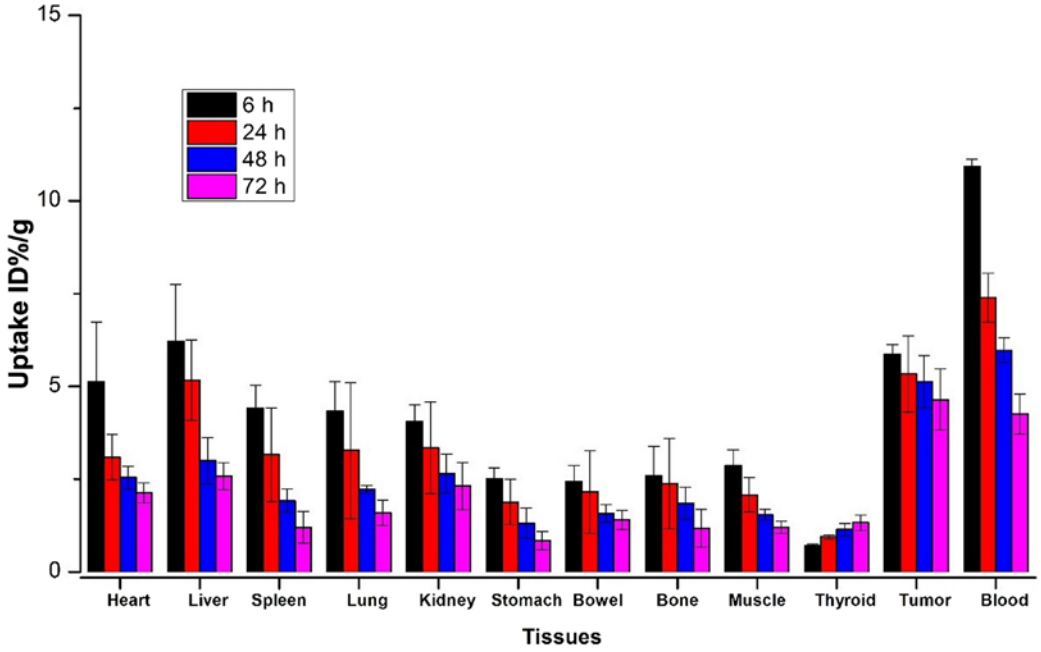

Figure 8. Biodistribution results for ^{131}I-anti-NRP-2 mAb in A549 xenogratfs. Data are expressed as %ID/g at various times after intravenous injection of ^{131}I-anti-NRP-2 mAb (n=4 for each group).

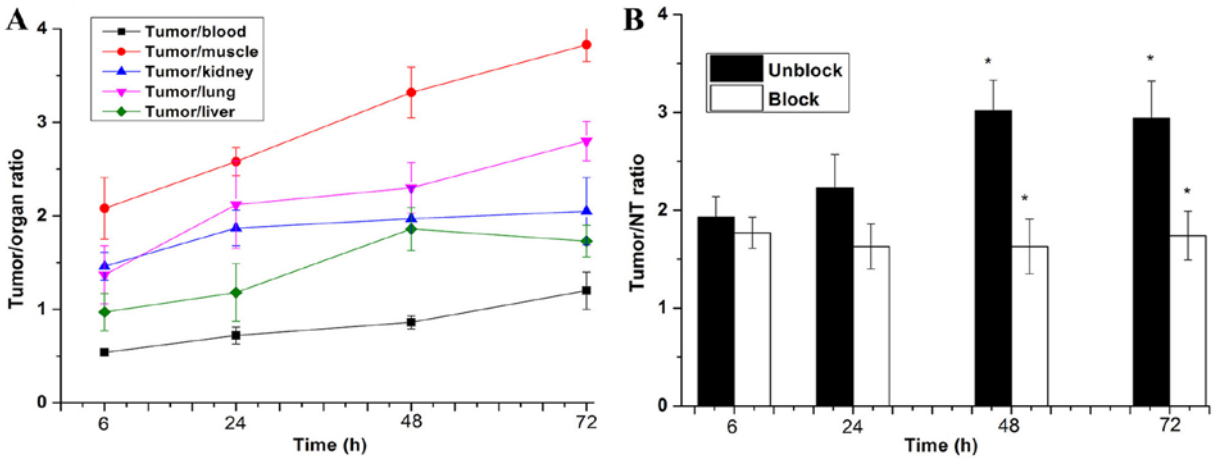

Figure 9. Tumor to normal organ ratios based on biodistribution for ^{131}I-anti-NRP-2 mAb in A549 xenogratfs (A), and tumor to contralateral muscle ratio (T/NT) based on SPECT imaging (B). *P<0.05, comparing of T/NT based on SPECT imaging between 0 μg (unblock) and 100 μg (block) dose at various times after injection with ^{131}I-anti-NRP-2 mAb.

tumor progression and metastasis (15-19). Recent evidence suggests that NRP-2 is important for therapy resistance by activating autophagy in different cancer types, including bladder cancer (21), prostate cancer (32) and pancreatic cancer (17), indicating that NRP-2 expression is a predictive marker for the outcome of cancer patients. Furthermore, inhibition of NRP-2 expression thus appears to be a promising approach for cancer therapy. Several NRP-2 targeting strategies, such as small interfering RNA (siRNA) (19), monoclonal antibodies (22) and small-molecule peptides (33), have shown some advantages, including inhibition of tumor lymphangiogenesis and angiogenesis, thereby restricting tumor metastasis and progression. Patients with cancer lesions that express NRP-2 may benefit from NRP-2 targeted therapy. Clinical trials have shown that there is an urgent unmet clinical need for the development of predictive biomarkers permitting patient selection for such therapy. Non-invasive molecular imaging, including SPECT imaging, is an ideal method, since it can offer a more accurate and real-time assay of NRP-2 expression, without such biopsy-associated pitfalls and the need of repetitive invasive biopsies. Therefore, to develop an imaging agent for NRP-2 expression is significantly important since our goal is to ultimately apply antibody-based SPECT probes for imaging patients.

The present study investigated the expression of NRP-2 in the human lung cancer cells. Consistent with previous studies (15,34), it was found that human lung adenocarcinoma A549 cells and tumor xenografts of A549 cells exhibited higher levels of NRP-2 expression than normal lung tissue. Nasarre *et al* (15) reported that in lung cancer

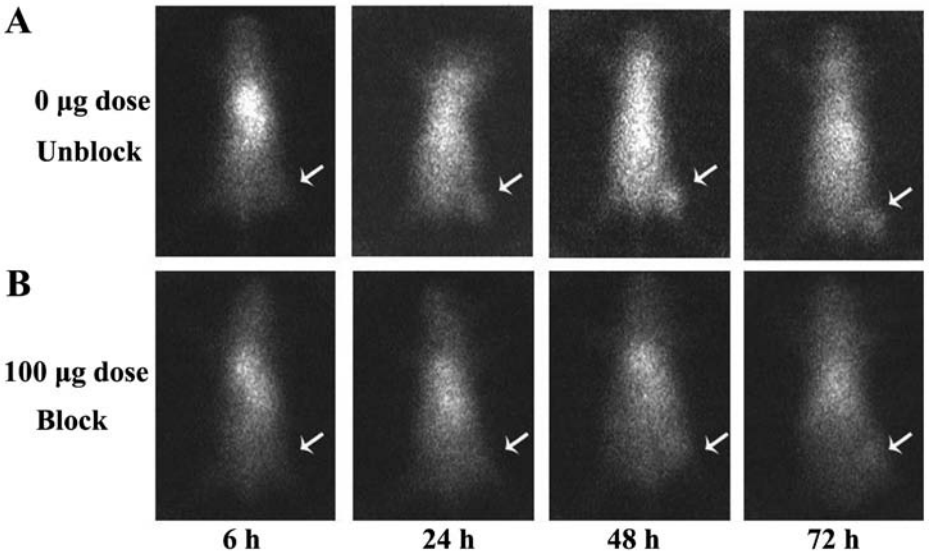

Figure 10. SPECT imaging of ^{131}I-anti-NRP-2 mAb in A549 xenograft models co-injected with 0 μg dose (A) and 100 μg dose [block (B)] of anti-NRP-2 mAb at 6, 24, 28 and 72 h after injection (n=4 for each group).

cells, NRP-2 is upregulated and contributes significantly to TGF-β-mediated epithelial-mesenchymal transition (EMT), which is fundamental process involved in tumor cell invasion and metastasis. In addition, in agreement with the report by Tomizawa *et al* (35), NRP-2 expression in H1299 cells is lower than that in 16HBE cells (human normal bronchial epithelial cells) since H1299 cells, derived from a lymph node metastasis of the lung from a patient who had received prior radiation therapy, have a homozygous partial deletion of the p53 gene, and lack expression of p53 protein, but can produce neuromedin B. These results demonstrated that NRP-2 may be a novel molecular target for lung adenocarcinoma diagnosis and therapy.

Due to their highly specific targeting ability, monoclonal antibodies (mAbs) have been considered attractive candidates for targeted therapy and diagnostics in a broad range of medical indications, but especially in oncology (36). Our previous studies showed that a novel anti-NRP-2 mAb, developed by our laboratory, can inhibit tumor proliferation, growth, and migration (unpublished data), indicating that anti-NRP-2 mAb may be an effective agent for NRP-2-targeted imaging and therapy. To further study anti-NRP-2 mAb imaging performance in targeting NRP-2, herein, we re-generated anti-NRP-2 mAb by hybridoma. This anti-NRP-2 mAb is confirmed to specifically bind to NRP-2 b1b2 domain and NRP-2 receptor on the surface of the A549 cells, but not NRP-1 b1b2 domain (Figs. 2, 3 and 5B), consistent with previous studies (22). SDS-PAGE (Fig. 4) indicated the successful production and purification (>95%) of anti-NRP-2 mAb sufficient for *in vitro* and *in vivo* cancer research.

Anti-NRP-2 mAb was labeled with ^{131}I by the chloramine-T method, and then measured the binding specificity and affinity to NRP-2. The probe ^{131}I-anti-NRP-2 mAb showed high binding affinity to the A549 cell NRP-2 with an IC_{50} of 96.6±1.44 nM (Fig. 7B), in agreement with the study by Parker and Vander Kooi (33). *In vitro* cell uptake experiments showed that ^{131}I-anti-NRP-2 had rapid accumulation in the A549 cells, and reached the highest value of 6.60±0.36% of applied activity at 180 min (Fig. 7A). This accumulation is NRP-2 specific receptor binding since the rapid cellular uptake of the tracer could be effectively blocked by cold anti-NRP-2 mAb (Fig. 7A), suggesting that labeling has not influenced the ability of anti-NRP-2 mAb to bind specifically to NRP-2. These results warranted further evaluation of the probe for *in vivo* NRP-2-targeted tumor imaging.

^{131}I-anti-NRP-2 mAb was also evaluated as a specific targeted radiotracer in A549 xenograft-bearing mouse models. The biodistribution data showed that ^{131}I-anti-NRP-2 mAb had a high tumor uptake, retention, and tumor to contralateral muscle ratio (T/NT) (Figs. 8 and 9). In addition, SPECT showed that the radioactive accumulation in the tumor site became visible from 6 h post-injection, and increased continually. Evaluation of the probe in mice demonstrated that ^{131}I-anti-NRP-2 mAb is a promising agent for NRP-2 imaging.

In this study, the liver, lung, spleen, blood and kidney showed high uptake at 6 h after administration. ^{131}I-anti-NRP-2 mAb was enriched more in the lung, liver and kidney, because of the moderate natural expression of NRP-1 in the lung and liver (37) and mAb metabolism through the liver and kidney. The high level of ^{131}I-anti-NRP-2 mAb in the blood and spleen is also possibly due to long circulating mAbs. Whereas, at 48 and 72 h after injection of ^{131}I-anti-NRP-2 mAb, with ^{131}I-anti-NRP-2 mAb clearance from blood, the level of the tumor uptake still remained higher than that in the other organs including the liver and blood. A moderate expression of the target in normal organ may appreciable influence the imaging results, especially when the target level in the tumor is low. After optimization of spiking doses to saturate the target expression in normal organ, increased tumor-normal ratio could be achieved (28,29). In the study, the *in vivo* NRP-2 binding specificity of ^{131}I-anti-NRP-2 mAb was also verified. When 100 μg of unlabeled anti-NRP-2 mAb was co-injected, uptakes in NRP-2 expression organs/tissues, such as the tumor, lung, and liver, were obviously reduced (Fig. 10B).

However, the characteristics of ^{131}I-monoclonal antibody, low tumor accumulation, slow clearance from the circulation,

and high energy iodine-131, may hamper its clinical applications. We have currently undertaken studies to improve these parameters. For example, the antibody fragments or anti-NRP-2 Affibody molecules and the way of labeling with low energy ^{99m}Tc or ^{111}In could increase rapidly NRP-2-positive tumor targeting ability and gain high imaging contrast within a short period after injection.

Imaging of NRP-2 expression *in vivo* may be not only be of value for treatment optimization of cancer patients, but also useful for identifying the sensitivity to chemotherapy in the patients with pancreatic cancer, bladder cancer, prostate cancer and lung cancer, that are resistant to chemotherapy, radio-chemotherapy, or radiotherapy through this mechanism, because NRP-2 overexpression increases VEGF-C/NRP-2 axis and β-catenin-dependent signaling. VEGF-C/NRP-2 axis induces autophagy to cancer cells from chemotherapeutic stress, and is also important to maintain an anti-apoptotic program in cancer cells during oxidative stress (21,32). Samuel *et al* (14) reported that knockdown of NRP-2 by an anti-NRP-2 antibody sensitized gastrointestinal cancer cells in 5-fluorouracil (5-FU) toxicity via β-catenin-dependent signaling. Thus, further research for imaging of NRP-2 expression has high clinical translational ability and will likely find broad application in patient therapy and management for targeting the expression of NRP-2 and cross-talk between Wnt/β-catenin and NRP-2 signaling.

In conclusion, an anti-NRP-2 monoclonal antibody was easily and successfully radiolabeled with iodine-131. The *in vitro* and *in vivo* study showed the potential of ^{131}I-anti-NRP-2 mAb as a promising SPECT probe for imaging NRP-2-positive tumors and encouraged further investigation. Nevertheless, since anti-NRP-2 mAb has a large molecular weight and an immunogenicity that may hinder its application in the clinic, it remains a great challenge to explore a novel small fragment of mAbs or Affibody molecules to improve imaging of NRP-2-expression.

Acknowledgements

This study was supported by grants from the National Natural Science Foundation of China (NSFC) (no. 81571707), program for the Training Young Talents of Fujian Health (no. 2014-ZQN-ZD-35), the Natural Science Foundation of Fujian (no. 2015J01519), the Technology Foundation for Selected Overseas Chinese Scholar, Ministry of Human Resources and Social Security of China (no. 2014-240) and the Scientific Research Foundation for the Returned Overseas Chinese Scholars, Ministry of Education of China (no. 2014-1685).

References

1. Takagi S, Tsuji T, Amagai T, Takamatsu T and Fujisawa H: Specific cell surface labels in the visual centers of *Xenopus laevis* tadpole identified using monoclonal antibodies. Dev Biol 122: 90-100, 1987.
2. Raimondi C and Ruhrberg C: Neuropilin signalling in vessels, neurons and tumours. Semin Cell Dev Biol 24: 172-178, 2013.
3. Prud'homme GJ and Glinka Y: Neuropilins are multifunctional coreceptors involved in tumor initiation, growth, metastasis and immunity. Oncotarget 3: 921-939, 2012.
4. Geretti E, Shimizu A and Klagsbrun M: Neuropilin structure governs VEGF and semaphorin binding and regulates angiogenesis. Angiogenesis 11: 31-39, 2008.
5. Geretti E and Klagsbrun M: Neuropilins: Novel targets for anti-angiogenesis therapies. Cell Adhes Migr 1: 56-61, 2007.
6. Chaudhary B, Khaled YS, Ammori BJ and Elkord E: Neuropilin 1: Function and therapeutic potential in cancer. Cancer Immunol Immunother 63: 81-99, 2014.
7. Plein A, Fantin A and Ruhrberg C: Neuropilin regulation of angiogenesis, arteriogenesis, and vascular permeability. Microcirculation 21: 315-323, 2014.
8. Sulpice E, Plouët J, Bergé M, Allanic D, Tobelem G and Merkulova-Rainon T: Neuropilin-1 and neuropilin-2 act as coreceptors, potentiating proangiogenic activity. Blood 111: 2036-2045, 2008.
9. Parker MW, Xu P, Li X and Vander Kooi CW: Structural basis for selective vascular endothelial growth factor-A (VEGF-A) binding toneuropilin-1. J Biol Chem 287: 11082-11089, 2012.
10. Kärpänen T, Heckman CA, Keskitalo S, Jeltsch M, Ollila H, Neufeld G, Tamagnone L and Alitalo K: Functional interaction of VEGF-C and VEGF-D with neuropilin receptors. FASEB J 20: 1462-1472, 2006.
11. Yuan L, Moyon D, Pardanaud L, Bréant C, Karkkainen MJ, Alitalo K and Eichmann A: Abnormal lymphatic vessel development in neuropilin 2 mutant mice. Development 129: 4797-4806, 2002.
12. Zhang Y, Liu P, Jiang Y, Dou X, Yan J, Ma C, Fan Q, Wang W, Su F, Tang H, *et al*: High expression of neuropilin-1 associates with unfavorable clinicopathological features in hepatocellular carcinoma. Pathol Oncol Res 22: 367-375, 2016.
13. Hey-Cunningham AJ, Markham R, Fraser IS and Berbic M: Dysregulation of vascular endothelial growth factors and their neuropilin receptors in the eutopic endometrium of women with endometriosis. Reprod Sci 20: 1382-1389, 2013.
14. Samuel S, Gaur P, Fan F, Xia L, Gray MJ, Dallas NA, Bose D, Rodriguez-Aguayo C, Lopez-Berestein G, Plowman G, *et al*: Neuropilin-2 mediated β-catenin signaling and survival in human gastro-intestinal cancer cell lines. PLoS One 6: e23208, 2011.
15. Nasarre P, Gemmill RM, Potiron VA, Roche J, Lu X, Barón AE, Korch C, Garrett-Mayer E, Lagana A, Howe PH, *et al*: Neuropilin-2 Is upregulated in lung cancer cells during TGF-β1-induced epithelial-mesenchymal transition. Cancer Res 73: 7111-7121, 2013.
16. Cao Y, Hoeppner LH, Bach S, E G, Guo Y, Wang E, Wu J, Cowley MJ, Chang DK, Waddell N, *et al*: Neuropilin-2 promotes extravasation and metastasis by interacting with endothelial α5 integrin. Cancer Res 73: 4579-4590, 2013.
17. Dallas NA, Gray MJ, Xia L, Fan F, van Buren G II, Gaur P, Samuel S, Lim SJ, Arumugam T, Ramachandran V, *et al*: Neuropilin-2-mediated tumor growth and angiogenesis in pancreatic adenocarcinoma. Clin Cancer Res 14: 8052-8060, 2008.
18. Dutta S, Roy S, Polavaram NS, Baretton GB, Muders MH, Batra S and Datta K: NRP2 transcriptionally regulates its downstream effector WDFY1. Sci Rep 6: 23588, 2016.
19. Gray MJ, Van Buren G, Dallas NA, Xia L, Wang X, Yang AD, Somcio RJ, Lin YG, Lim S, Fan F, *et al*: Therapeutic targeting of neuropilin-2 on colorectal carcinoma cells implanted in the murine liver. J Natl Cancer Inst 100: 109-120, 2008.
20. Dutta S, Roy S, Polavaram NS, Stanton MJ, Zhang H, Bhola T, Hönscheid P, Donohue TM Jr, Band H, Batra SK, *et al*: Neuropilin-2 regulates endosome maturation and EGFR trafficking to support cancer cell pathobiology. Cancer Res 76: 418-428, 2016.
21. Keck B, Wach S, Taubert H, Zeiler S, Ott OJ, Kunath F, Hartmann A, Bertz S, Weiss C, Hönscheid P, *et al*: Neuropilin-2 and its ligand VEGF-C predict treatment response after transurethral resection and radiochemotherapy in bladder cancer patients. Int J Cancer 136: 443-451, 2015.
22. Caunt M, Mak J, Liang WC, Stawicki S, Pan Q, Tong RK, Kowalski J, Ho C, Reslan HB, Ross J, *et al*: Blocking neuropilin-2 function inhibits tumor cell metastasis. Cancer Cell 13: 331-342, 2008.
23. Sun H, England CG, Hernandez R, Graves SA, Majewski RL, Kamkaew A, Jiang D, Barnhart TE, Yang Y and Cai W: ImmunoPET for assessing the differential uptake of a CD146-specific monoclonal antibody in lung cancer. Eur J Nucl Med Mol Imaging 43: 2169-2179, 2016.
24. Yang Y, Chen N, Li Z, Wang XJ, Wang SY, Tingwu, Luo FH and Yan JH: Preparation, purification, and identification of a monoclonal antibody against NRP2 b1b2 domain. Monoclon Antib Immunodiagn Immunother 34: 354-359, 2015.
25. Su X, Chen Q, Chen W, Chen T, Li W, Li Y, Dou X, Zhang Y, Shen Y, Wu H, *et al*: Mycoepoxydiene inhibits activation of BV2 microglia stimulated by lipopolysaccharide through suppressing NF-κB, ERK 1/2 and toll-like receptor pathways. Int Immunopharmacol 19: 88-93, 2014.

26. Dou X, Yan J, Zhang Y, Liu P, Jiang Y, Lv S, Zeng F, Chen X, Wang S, Zhang H, *et al*: SPECT imaging of neuropilin receptor type-1 expression with ^{131}I-labeled monoclonal antibody. Int J Oncol 49: 961-970, 2016.
27. Guo Z, Gao M, Zhang D, Li Y, Song M, Zhuang R, Su X, Chen G, Liu T, Liu P, *et al*: Simultaneous SPECT imaging of multi-targets to assist in identifying hepatic lesions. Sci Rep 6: 28812, 2016.
28. Su X, Cheng K, Liu Y, Hu X, Meng S and Cheng Z: PET imaging of insulin-like growth factor type 1 receptor expression with a 64Cu-labeled Affibody molecule. Amino Acids 47: 1409-1419, 2015.
29. Su X, Cheng K, Jeon J, Shen B, Venturin GT, Hu X, Rao J, Chin FT, Wu H and Cheng Z: Comparison of two site-specifically (18)F-labeled affibodies for PET imaging of EGFR positive tumors. Mol Pharm 11: 3947-3956, 2014.
30. Guo Z, Gao M, Song M, Shi C, Zhang P, Xu D, You L, Zhuang R, Su X, Liu T, *et al*: Synthesis and evaluation of (99m)Tc-labeled dimeric folic acid for FR-targeting. Molecules 21: E817, 2016.
31. Chen H, Chédotal A, He Z, Goodman CS and Tessier-Lavigne M: Neuropilin-2, a novel member of the neuropilin family, is a high affinity receptor for the semaphorins Sema E and Sema IV but not Sema III. Neuron 19: 547-559, 1997.
32. Stanton MJ, Dutta S, Zhang H, Polavaram NS, Leontovich AA, Hönscheid P, Sinicrope FA, Tindall DJ, Muders MH and Datta K: Autophagy control by the VEGF-C/NRP-2 axis in cancer and its implication for treatment resistance. Cancer Res 73: 160-171, 2013.
33. Parker MW and Vander Kooi CW: Microplate-based screening for small molecule inhibitors of neuropilin-2/vascular endothelial growth factor-C interactions. Anal Biochem 453: 4-6, 2014.
34. Jubb AM, Sa SM, Ratti N, Strickland LA, Schmidt M, Callahan CA and Koeppen H: Neuropilin-2 expression in cancer. Histopathology 61: 340-349, 2012.
35. Tomizawa Y, Sekido Y, Kondo M, Gao B, Yokota J, Roche J, Drabkin H, Lerman MI, Gazdar AF and Minna JD: Inhibition of lung cancer cell growth and induction of apoptosis after reexpression of 3p21.3 candidate tumor suppressor gene SEMA3B. Proc Natl Acad Sci USA 98: 13954-13959, 2001.
36. Khan AH and Sadroddiny E: Licensed monoclonal antibodies and associated challenges. Hum Antibodies 23: 63-72, 2015.
37. Aung NY, Ohe R, Meng H, Kabasawa T, Yang S, Kato T and Yamakawa M: Specific neuropilins expression in alveolar macrophages among tissue-specific macrophages. PLoS One 11: e0147358, 2016.